Proceedings of IMECE04
2004 ASME International Mechanical Engineering Congress and Exposition
November 13-20, 2004, Anaheim, California USA

IMECE2004-59661

EXPERIMENTAL CHARACTERIZATION AND SIMULATION OF THREE DIMENSIONAL PLASTIC DEFORMATION INDUCED BY MICROSCALE LASER SHOCK PEENING

Hongqiang Chen
Department of Mechanical Engineering
Columbia University
New York, NY 10027 USA
hc2008@columbia.edu

Jeffrey W. Kysar
Department of Mechanical Engineering
Columbia University
New York, NY 10027 USA
jk2079@columbia.edu

Y. Lawrence Yao
Department of Mechanical Engineering
Columbia University
New York, NY 10027 USA
yly1@columbia.edu

Youneng Wang
Department of Mechanical Engineering
Columbia University
New York, NY 10027 USA
yw2119@columbia.edu

ABSTRACT

Different experimental techniques and 3D FEM simulations are employed to characterize and analyze the three dimensional plastic deformation and residual strain/stress distribution for single crystal Aluminum under microscale laser shock peening assuming finite geometry. Single pulse shock peening at individual locations was studied. X-ray micro-diffraction techniques based on a synchrotron light source affords micron scale spatial resolution and is used to measure the residual stress spatial distribution along different crystalline directions on the shocked surface. Crystal lattice rotation due to plastic deformation is also measured with electron backscatter diffraction (EBSD). The result is experimentally quantified and compared with the simulation result obtained from FEM analysis. The influence of the finite size effect, crystalline orientation are investigated using single crystal plasticity in FEM analysis. The result of the 3D simulations of a single shock peened indentation are compared with the FEM results for a shocked line under 2D plain strain deformation assumption. The prediction of overall character of the deformation and lattice rotation fields in three dimensions will lay the ground work for practical application of μLSP.

KEYWORDS: Laser shock peening, Electron backscatter diffraction, Single crystal plasticity, X-ray micro-diffraction

1 INTRODUCTION

Recently, laser shock processing of polycrystalline aluminum and copper using a micron sized laser beam has been studied [1,2]. It has been shown that micron-scale laser shock peening (μLSP) can efficiently induce a compressive residual stress distributions in bulk metal targets as measured by X-ray diffraction with micron-level spatial resolution [3] and calculated through finite element analysis (FEM) simulations [4]. Thus, microscale laser shock peening (μLSP) can be used to manipulate the residual stress distributions in metal structures over regions as small as a few microns and thus improve the reliability of micro-devices.

Microscale laser shock peening, has been the subject of several experimental studies to characterize the induced stress and deformation fields, in parallel with FEM studies [3,5]. The X-ray micro-diffraction technique was used to measure the spatially resolved residual stress state; the resulting diffraction peak profiles were quantified and explained in terms of a heterogeneous dislocation cell structure [6] in laser shock peened Al and Cu single crystals. From the work of Kysar and Briant [7], electron backscatter diffraction (EBSD) was used to investigate crystal lattice rotation caused by plastic deformation during laser shock peening in single crystal Al and Cu [3,5]. Crystal lattice rotation on and below the micro-scale laser shock peened sample surface was measured. The measured lattice rotation makes it possible to estimate the lattice curvature, and hence, the geometrically necessary dislocation density [8] so that length scale effects at the micron scale can be investigated. Single crystal plasticity simulations along with EBSD measurements were applied to study plastic deformation induced by a channel die [9] and μLSP [5].

Previous studies of uLSP employed highly ideal geometries to simplify the experimental characterization and

facilitate FEM simulation. This was done by shock peening along a certain crystalline direction on the sample surface to achieve an approximate two-dimensional deformation state [5]. A 2-D FEM simulation was performed using the highly simplified assumptions of ideal plastic behavior in a single crystal under quasi-static plane strain conditions, thus neglecting even the three-dimensional effects. Nevertheless, the simulations were able to capture the salient features of the measured deformation field. Apparently, then, the anisotropic plastic behavior of the material plays a very important role in the process. Laser shock peening is an inherently 3-D process so it is necessary to characterize a single laser shock peen, as well.

In this paper, the micro-diffraction technique and EBSD are used to estimate the residual stress spatial distribution and measure lattice rotation associated with μLSP along different crystalline directions on the shocked sample surface. In additional, three dimensional FEM simulations are carried out to analyze the plastic deformation and strain/stress states for single crystal aluminum under microscale laser shock peening. Single and multiple pulses at individual locations were considered. The influence of the finite size effect, crystalline orientation and anisotropic plastic behavior of the single crystal are coupled into the single crystal plasticity in FEM analysis. 3D simulation result for a single peened point is compared with the result for a shocked line under 2D plain strain deformation assumption. These results lay the ground work for much more detailed simulations as well as for practical applications of μLSP, and is largely a continuation of Chen, et al. [5].

2 EXPERIMENTS

Several different methods were employed in the experiment to characterize the shock peened regions. Atomic force microscopy (AFM) was used to measure the deformation geometry on the shocked surfaces. X-ray microdiffraction and the sub-profile method were applied to estimate the shock induced residual stress state on the shocked surface. Moreover, the lattice rotation was characterized by electron backscatter diffraction (EBSD) to measure crystallographic orientation as a function of position.

2.1 Sample geometry and laser shock peening conditions

A frequency tripled Q-switched Nd:YAG laser ($\lambda = 355\ nm$) in TEM_{00} mode was used in the laser shock peening as illustrated in Fig. 1. In order to achieve a three dimensional deformation state, a single laser pulse was applied on the sample surface with a 50 ns pulse duration to generate a "dent-like" shocked region. The laser beam diameter was 12 μm and laser intensity was approximately $4GW/cm^2$. Further details of the micro-scale LSP setup are given in Zhang and Yao [1,2].

Fully-annealed single crystals of pure aluminum (grown by the seeded Bridgman technique) were used in the experiment. Aluminum was chosen because it is routinely used in micro-devices due to its good mechanical and electrical properties. The (001), (110) and (111) planes were identified by Laue X-ray and the sample, as shown in Fig. 1, was cut to shape using a Wire Electrical Discharge Machining (EDM). The coordinate systems used throughout this paper are indicated in Fig. 1 and defined as follows: Z-axis is parallel to crystal direction of [110], X-axis is parallel to [001] direction and Y-axis is parallel to $[1\bar{1}0]$ direction. The $(1\bar{1}0)$ surface of the crystal was laser-shock peened. Single crystals are used in this study for two main reasons. First, the grain size of many materials is approximately 10um, which is about the same size as the laser spot. Therefore, an isotropic constitutive assumption is not adequate to understand the process. Thus the response of an anisotropic material to μLSP is of direct interest. Second, a single crystal is anisotropic, nut homogeneous, which greatly facilitate experimental characterization. Therefore, single crystals are candidates for fundamental and systematic study of material response to μLSP. Sample preparation details can be found in [1-3, 5]

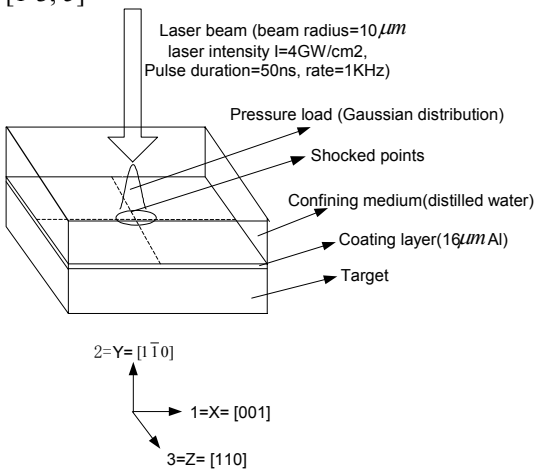

Fig. 1 Sample geometry and shock peening condition of single crystal Al (110)

2.2 Deformation geometry measured by AFM

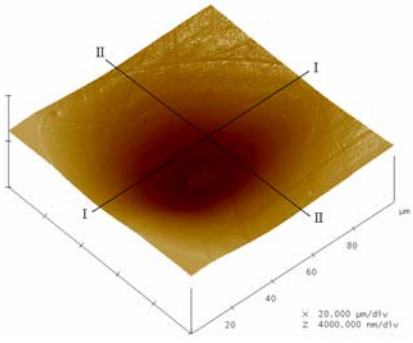

(a)

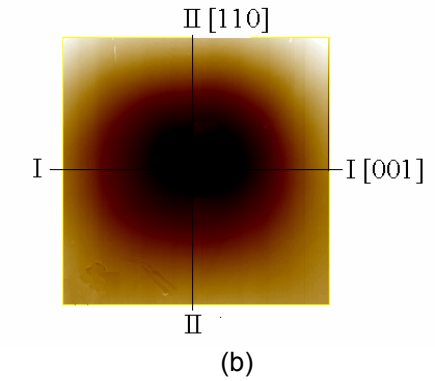

(b)

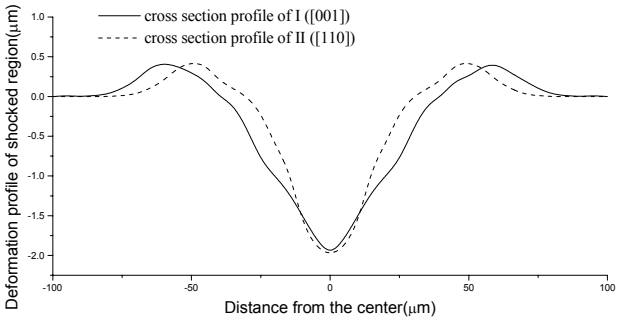

(c)

Fig. 2 Typical surface profile of shocked region from AFM
(a) 3-D view (b) Top view (c) Cross section profile

The shocked region geometry has been determined by means of atomic force microscopy (AFM, Digital Instruments Nanoscope Inc.) observations. Using non-contact mode, a typical 3D geometry of the shocked region measured is seen in Fig. 2(a); the scan area is 100×100μm and 512 measurements were made along each direction. As is evident, the depth of the shocked region is around 2.5μm with diameter close to 80μm. In order to study the material response in different crystalline direction. (I and II in Fig. 2(b)). The geometry profile of different cross-section measured by AFM in Fig. 2(c). It can be seen that the general trend of profile along different directions is the same, however, the lateral extent along I (<001>direction) is larger than that in II (<110> direction) which may caused by the anisotropic property of single crystal. Also there pile-up exists around the shocked peen due to the incompressibility assumption.

2.3 X-ray microdiffraction measurement

2.3.1 X-ray microdiffraction measurement scheme

X-ray beams from synchrotron radiation sources (from beamline X20A at National Synchrotron Light Source at Brookhaven National Lab) were used in this study because the extreme intensities allow a short sampling time and further, the x-ray can be focused by a tapered glass capillary to spot sizes as small as 3 microns. Complete details of the X-ray microdiffraction experiment can be found in [3].

In order to spatially resolve the residual stress induced by μLSP, measurements were made in a grid pattern over the shocked region as shown in Fig. 3. The spacing between adjacent measurement points is 5 μm when within 20 μm of the shock center and is 10 μm at distances greater than 20μm from the shock center. At each position, the corresponding X-ray diffraction profile is recorded and repeated for each scan line. The shape of the profile and its shift can be interpreted in terms of the residual stress state, as will be discussed in the next section.

For *FCC* metals, the diffraction structure factor for (110) is zero and the reflections are absent [10], so the (220) reflections are chosen for X-ray diffraction measurement. For the Al (110) sample in Fig. 1, the crystalline structure has special directions along lines I, II and III which corresponds, respectly, to [001], [110] and [111] directions. In order to study the anisotropic behavior of single crystal which undergo μLSP, the X-ray profiles along those directions were investigated, in addition to making measurements over the grid.

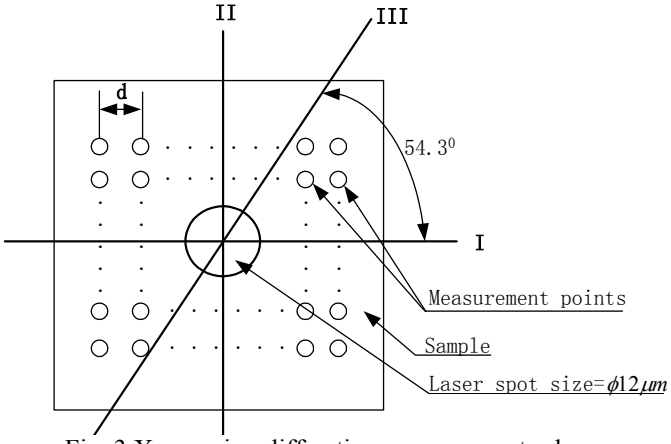

Fig. 3 X-ray microdiffraction measurement scheme
(I: [001] direction, II: [110] direction, III: [111] direction)

2.3.2 Diffraction profile analysis

Sub-profile analysis using the composite model by Ungar [6] was employed to interpret the diffraction profiles, as in [3]. After obtaining the X-ray diffraction profile, the asymmetric line profiles I were assumed to be composed of two components I_w and I_c, where I_w is attributed to the cell-wall material and I_c to the cell-interior material. The lateral residual stress in the sample surface plane can be estimated based on this assumption.

Fig. 4 shows the typical three dimensional spatial distribution of the measured X-ray diffraction intensity profiles of the (220) Bragg reflection along line I ([001] direction). The salient features of these line profiles can be summarized as follows:

(a) When the measure point moved across the shock center from left to right in Fig. 4, the line profiles change distinctively from a single symmetric peak to asymmetry with a second peak becoming visible, and finally return to a single symmetric peak. It is clear that after shock peening, the X-ray profile was significantly broadened and became asymmetric compared to unshocked region.

(b) At ±100μm and beyond, the measured profile peak value is almost at the theoretical angle, which in turn represents the shock free regions, which represents a diffraction profile referred to type A, herein. As the shock is approached, the main peak shifts towards larger diffraction angles, while a second peak pops up towards smaller diffraction angle (type B diffraction profile); for the region near the dent center, the main peak shifts towards smaller diffraction angles, while a second peak pops up towards larger diffraction angle (type C diffraction profile).

The type B profiles indicate a tensile residual lateral stress state and the type C profiles indicate a compressive residual stress state. The striking transition from type C to type B away from the shock region indicates a fundamental change in the residual stress state independent of sub profile interpretation. The X-ray diffraction profiles show similar patterns along different crystalline directions (line I and line II). However, for the broadened asymmetric profile, the type A profile is more significant in (110) direction than (111) and (001) direction while type B profile is dominant along [001] direction. The area

with broadened and shifted profiles is smallest in (110) direction, followed by (111) and (001) direction.

Interpretation of diffraction profiles in highly deformed regions is often ambiguous so the results are not clear-cut. Nevertheless it should be emphasized that qualitative differences of the diffraction profiles as a function of position relative to the shocked region, strongly suggest a transition from compressive to tensile residual stress state, independent of the specific methods used to interpret the diffraction profiles quantitatively.

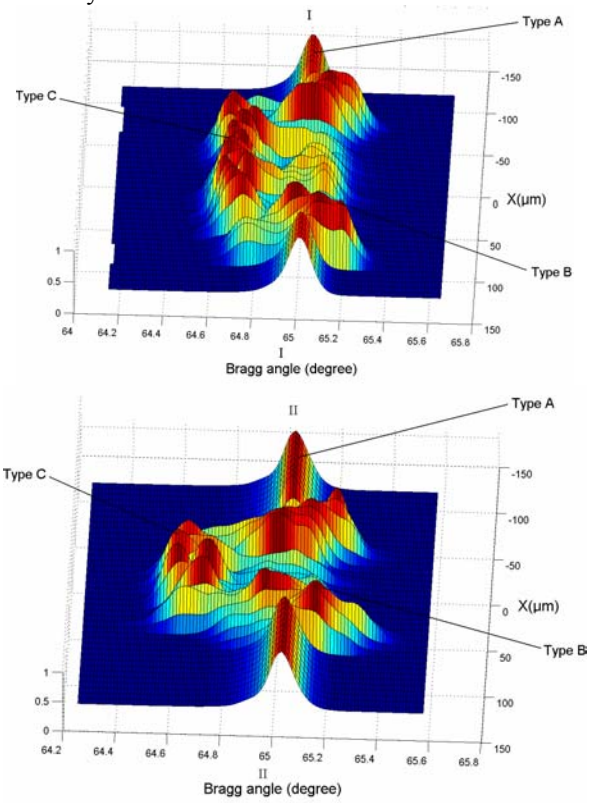

Fig. 4 Typical X-ray diffraction profile spatial distribution along line I [001] and II [110]

2.3.3 Approximate residual stress distribution from X-ray measurement

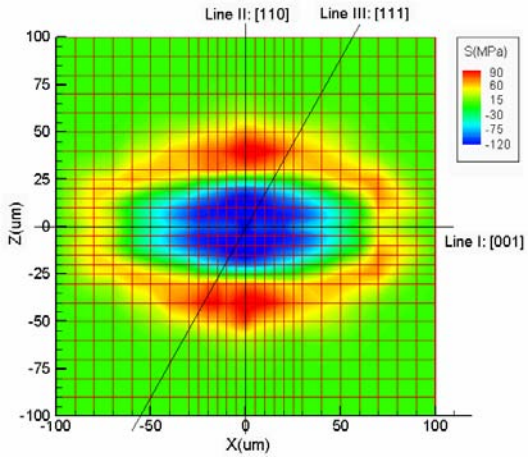

Fig. 5 Surface residual stress distribution from X-ray microdiffraction

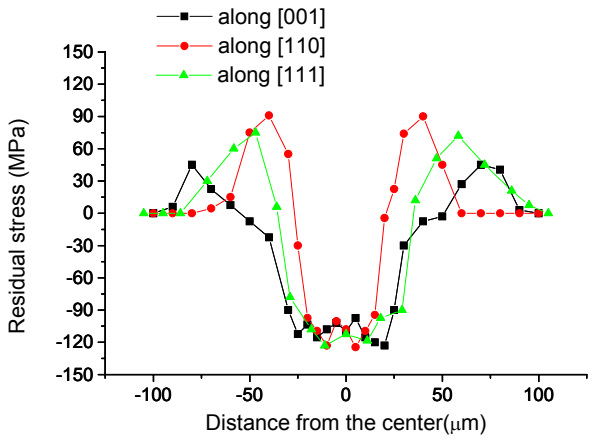

Fig. 6 Lateral residual stress distribution from X-ray diffraction measurement for Al (110) sample

After obtaining the X-ray diffraction profile at different positions in shocked region, the lateral residual stress on sample surface can be estimated using the methods from Chen, et al. [3] and the spatial distribution across the shocked region plotted as in Fig. 5. The stress can be considered to be average stress in the region sampled by X-ray diffraction. A compressive residual stress is generated near the center of shocked region bordered by a region of tensile stress. Although the laser spot size is only 12μm, the high shock pressure in μLSP can generate significant compressive residual stresses over a much larger region. The compressive stress is estimated to have a maximum value of –120MPa near the center and cover an ellipse-like region which extends ±60μm along [001] direction and ±25μm along [110] direction from the center. The maximum residual tensile stress is estimated to be +90MPa and occurs in [110] direction approximately 40μm away from the shock center while the minimum residual tensile stress exists in [001] direction. In order to study the influence of crystal direction on residual stress distribution, Fig. 6 shows the estimated lateral residual stress distribution on Al (110) sample surface along [001], [111] and [110] direction. The distributions show similar patterns for different directions. Compressive residual stress exists in the shocked dent center and tensile stress exists at the outer range of dent. Again, the compressive residual stress extends further in the [001] than the [110].

2.4 EBSD measurement of lattice rotation

2.4.1 EBSD measurement scheme

Electron backscatter diffraction (EBSD) is a diffraction technique for obtaining crystallographic orientation with sub-micron spatial resolution from bulk samples or thin layers in the scanning electron microscope. EBSD is used to investigate crystal lattice rotation caused by plastic deformation during high-strain rate laser shock peening in single crystal aluminum and copper sample of $(1\bar{1}0)$ and (001) orientation [5], where new experimental methodologies were employed to enable measurement of the in-plane lattice rotation under approximate plane strain conditions. For the single dent shock peening, both in-plane and out-of-plane lattice rotation need to be

investigated to fully understand the 3-D plastic deformation and anisotropic property of single crystal under μLSP.

EBSD measurement was performed on the sample surface and over a region (150x150μm) larger than the shock peen. The EBSD data was collected using a system supplied by HKL Technology and attached to a JEOL JSM 5600LV scanning electron microscope. All data were acquired in the automatic mode, using external beam scanning and employing a 1μm step size. The EBSD results from each individual scan comprise data containing the position coordinates of electron beam along with the three Euler angles, which describe the orientation of the particular interaction volume relative to the orientation of the specimen in the SEM. This information allows the in-plane and the out-of-plane lattice rotations to be calculated relative to the known undeformed crystallographic orientation, which serves as the reference state.

2.4.2 Lattice rotation field from EBSD

As discussed in [5], the crystalline orientation will change after laser shock peening due to the plastic deformation. Fig. 7 illustrates a crystal orientation map obtained from EBSD, which describes the orientation difference (misorientation angle) before and after μLSP for the shocked region on Al (110) sample top surface (150x150μm). In this color contour, the green region corresponds to the shock free region since there is no change from the original crystal orientation. The red grayscales indicate a larger deviation of the <110> crystal axis from the sample surface normal and up to 5 degree. It is interesting that the contour distribution is approximately two-fold symmetric about the X and Z axis and the maximum misorientation occurs about 10μm away from the center and the overall region with significant orientation change is a ellipse-like with major axis about 80μm along the [001] direction and minor axis about 50μm along the [110] direction. The overall shape is consistent with the surface profile as measured by AFM measurement in Fig. 2. Thus, the misorientation contour indicates the affected region of plastic deformation in μLSP.

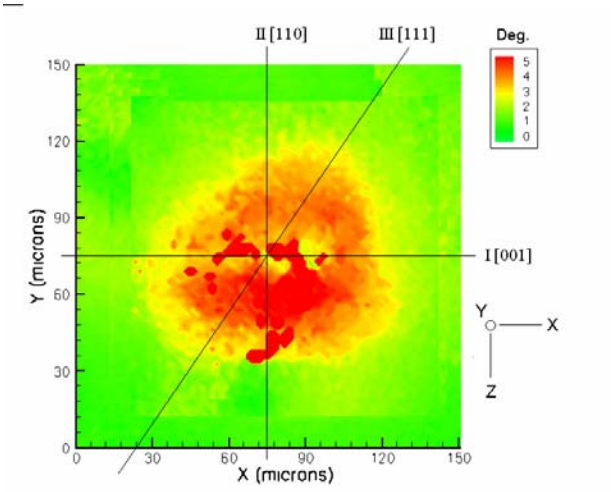

Fig. 7 Crystal misorientation angle distribution on sample surface

The misorientation angle, however, only shows the angular deviation between the <110> crystal axis after μLSP and the original surface normal before μLSP. Actually, the EBSD results from each individual scan comprise data containing the position coordinates and the three Euler angles ϕ_1, φ, ϕ_2 From which the corresponding α,β,γ angles around the fixed X, Y, Z axis can be calculated to study the 3-D lattice rotation.

Fig. 8(a-c) shows the lattice rotation around X, Y, Z axis separately for Al (110) sample from EBSD measurement. In order to study the anisotropic characteristics, the lattice rotation distribution along three typical crystal direction <001>, <110> and <111> are compared, shows significant anisotropy. The lattice rotation is mainly about the Z axis along <001> direction and about X axis along <110> direction. In <111> direction, both significant lattice rotation around X and Z axis are observed. For rotation about axis Y (surface normal), the value is almost zero along all three directions which indicates the lattice rotation around surface normal is very small after μLSP. In <001> direction, the lattice rotation around X axis is ±4° between ±40μm from the center of shocked region and the rotation direction is anti-symmetric on both side of shocked center. The lattice rotation distribution along the <110> direction is around ±4° anti-symmetric on both side of shocked center. However, the rotation is mainly about Z axis and the extent is around ±60μm from the center of shocked region which is larger than that in <001> direction. In <111> direction, both rotation around X and Z axis is observed and the anti-symmetric value is ±4° between ±50μm from the center of shocked region.

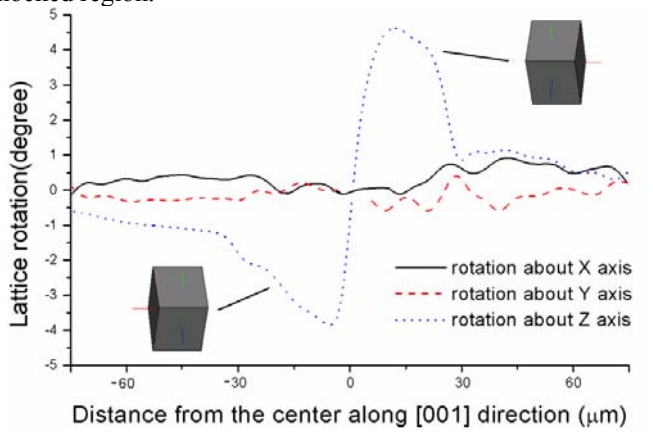

(a)

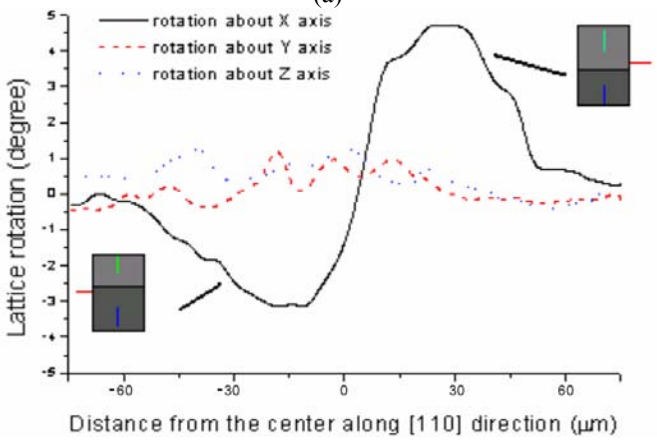

(b)

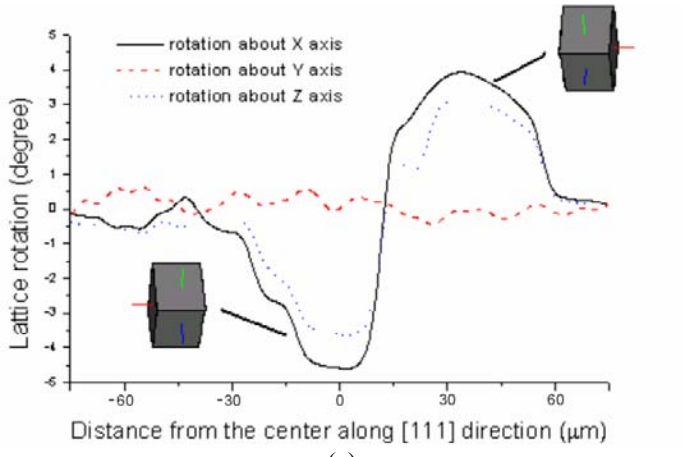

(c)

Fig. 8 Crystalline orientation change on sample surface

3. SIMULATIONS

3.1 Three dimensional FEM simulations

In this section, 3D FEM analyses were carried out to analyze the material response for single crystal Aluminum under μLSP. Instead of assuming a two-dimensional deformation state, the material deformation is considered as full three dimensional problem. Based on the theory of [11], a user-material subroutine (UMAT) for single crystal plasticity written by Huang [12] and modified by Kysar [13] is incorporated into the finite element analysis using the general purpose finite element program ABAQUS/Standard. The details about the single crystal plasticity can be found in [5]. The simulation is a two-step quasi-static loading and unloading process corresponding to the shock peening and relaxation processes. Only a quarter of the shocked sample need be computed due to sample geometric symmetry, and the selected computation domain is a 300 micron scale. In the simulation, 11, 22 and 33 direction are chosen as [001], [110] and $[1\bar{1}0]$ direction which correspond to the X, Y and Z coordinates in Figure 1. The typical von mises stress distribution through simulation is shown in Fig. 9. The loading conditions of the 3D model are as follows. On top surface (1-3 plane), the spatially non-uniform shock pressure with a Gaussian spatial distribution with its $1/e^2$ radius equals to $\sqrt{2}R$ is applied, where R is the radius of plasma (Zhang and Yao, 2000a). Let x and z be thedistancefrom the center of the laser beam along 1 and 3 directions, the spatially non-uniform shock pressure $P(x, z)$ is then given as

$$P(x,z) = P_0 \exp(-\frac{x^2 + z^2}{2R^2}) \qquad (1)$$

on the shocked surface. P_0 is the peak value of shock pressure and the plasma radius R=6μm here. In order to make a dimensionless analysis, all simulation results are normalized as the function of two dimensionless parameters $(P_0 / \tau_{CRSS}, x / R)$.

Due to the geometric symmetry, symmetric boundary conditions are applied on 1-2 and 2-3 plane and the bottom surface is fixed in position, while all the other side surfaces are traction free. On the top surface, surface traction equals the applied shock pressure,. In order to eliminate the "volume-locking" that occurs in plastic deformation simulation, 8-node linear brick elements with reduced integration and hourglass stiffness control were used.

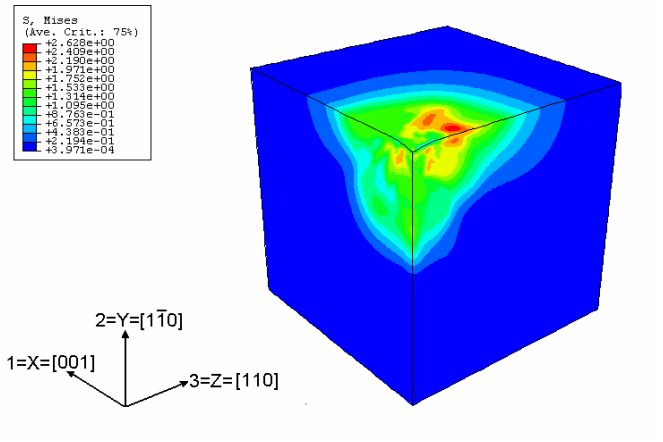

Fig. 9 Typical 3-D FEM simulation result, only quarter of the sample is simulated due to symmetry along X and Z axis (200×200×200μm). Deformation in the shocked region is magnified by a factor of 5 for viewing clarity.

3.2 Deformation geometry from FEM simulation

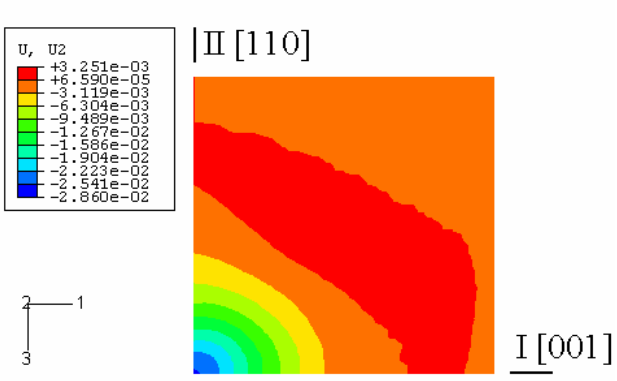

(a)

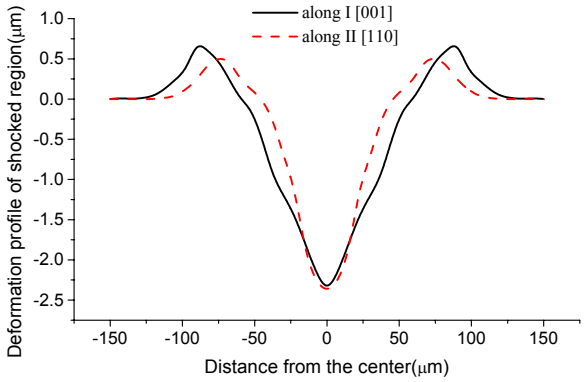

(b)

Fig. 10 Depth displacement distribution on sample surface from FEM simulation
(a) Depth deformation contour (150×150μm) (b) Depth distribution along line I and II

Fig. 10(a) shows the deformation depth distribution on the shocked surface predicted by 3-D FEM simulation. The red region corresponds approximately to the material pile up which is positive and the blue region corresponds the maximum depth of shocked region. It is clear that the deformation is not axisymmetric due to the anisotropic property of single crystal. Fig. 10(b) shows the predicted surface profile along line I and II. The distribution is similar with the AFM measurements of that in Fig. 2. Thus, the typical deformation geometry under uLSP is not a circular but an ellipse-like dent. Deformation extends farther along [001] direction than nalong the [110] direction.

The difference in extent of the shocked region in the [001] and [110] directions is related either to the anisotropic elasticity or the anisotropic plastic behavior, or both. We first consider the elastic behavior. For a cubic crystal, the compliance matrix only has three independent component S_{11}, S_{12}, S_{44}. The Young's modulus along 001 and 110 direction is

$$E_{[001]} = \frac{1}{S_{11}} \tag{2}$$

and $$E_{[110]} = \frac{2}{S_{11} + S_{12} + S_{44}/2} \tag{3}$$

Given the S_{11}=1.57, S_{12}=-0.57, S_{44}=3.54, $E_{[001]}$=0.637, $E_{[110]}$=0.722. Thus, the Young's modulus along [110] direction is somewhat greater than that in [001] direction, which may account for some of the difference.

In order to study the plastic an isotropic character in detail, the Schmidt factor of each active slip systems needs to be investigated. Suppose the loading direction is *l*, the slip plane normal is *n*, the slip direction is *s*, the Schmidt factor can be represented as $\cos\phi \times \cos\lambda = (n \cdot l) \times (s \cdot l)$, where ϕ is the angle between *n* and *l* and λ is the angle between *s* and *l*. The twelve slip systems in FCC Al are as follows and the loading direction is $[1\bar{1}0]$ as seen in Fig. 1.

Table 1

Slip plane *n*	Slip direction *s*	Schmidt factor for loading direction l=$[1\bar{1}0]$
(111)	$[\bar{1}10]$ $[10\bar{1}]$ $[0\bar{1}1]$	0 0 0
$(\bar{1}11)$	$[110]$ $[101]$ $[0\bar{1}1]$	0 $-1/\sqrt{6}$ $-1/\sqrt{6}$
$(1\bar{1}1)$	$[110]$ $[10\bar{1}]$ $[011]$	0 $1/\sqrt{6}$ $-1/\sqrt{6}$
$(11\bar{1})$	$[\bar{1}10]$ $[101]$ $[011]$	0 0 0

As seen in Table 1, for uniaxial loading along $[1\bar{1}0]$ direction, four of the twelve slip systems will be actived simultaneously since the magnitude of Schmidt factors are the same. As is well-known, six strains are necessary to specify an arbitrary strain state. The assumption of constant volume for plastic strain requires that the trace of the plastic strain tensor be zero. As a consequence, there are only 5 independent components of plastic strain so that five active slip systems are needed to achieve any arbitrary ε_{ij}. Since only four slip systems are activated in the present case, an arbitrary deformation state can not be attained. Rice [14] showed that the four slip systems under question can combine to form two effective slip systems which act in the (110) plane when they are activated in equal amounts. An arbitrary deformation state within that plane can be achieved because under plane strain condition there are only two independent plastic strain components and two slip systems. Thus, the shock loading generates a predominately plane deformation state in (110) plane, which is along the direction of line I [001]. Therefore, plastic deformation along [001] direction (line I) is much easier than that in [110] direction (line II), which accounts for the ellipse-like structure of the shocked region.

3.3 Approximate residual stress distribution from simulation

Through 3-D FEM simulation, the distribution of residual stress induced by μLSP can be studied and compared with X-ray measurement result which can be considered as the average stress along a certain depth below sample surface.

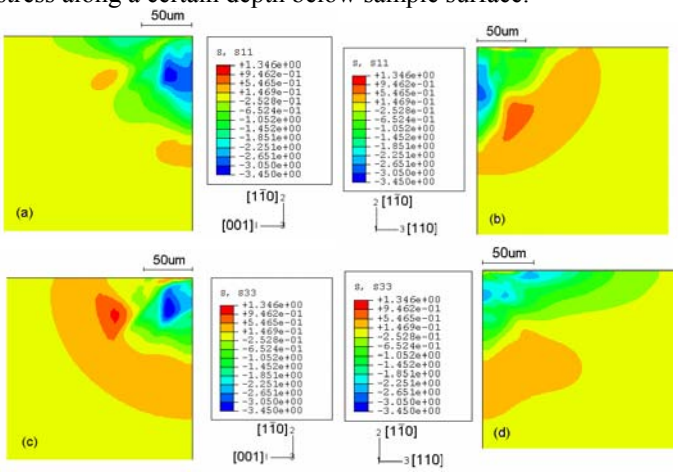

Fig. 11 FEM simulation of residual stress distribution at different cross section
(Axis 1: [001] direction, Axis 2: [1-10] direction, Axis 3: [110] direction)
(a) σ_{11} on 12 plane, (b) σ_{11} on 23 plane,
(c) σ_{33} on 12 plane, (d) σ_{33} on 23 plane

Fig. 11 shows the residual stress distribution in 11 and 33 direction which is parallel to the sample surface. It is clear that the magnitude and sign of residual stress is similar for σ11 and σ33 and compressive residual stress is encompassed by the tensile stress due to the force equilibrium. In the sub-profile analysis of X-ray diffraction profile, it is assumed that bi-axis stress state exists in sample surface and the calculated lateral residual stress is an approximation for σ11 and σ33. In order to study the anisotropic property of single crystal under μLSP, the σ11, σ33 distribution in different cross section 12 and 23 are shown in Fig 11 (a)-(d). In cross section 12, if we consider

σ11 and σ33 together, the magnitude of compressive stress is around three times the tensile stress and occurs from the center to 40 μm away. The tensile stress occurs from 80 μm away from the center and extend to 100μm. This result is consistent with the lateral residual stress distribution along 11 direction by X-ray measurement. In cross section 23, the magnitude of compressive stress and the lateral extent is smaller than that in 12 plane, which is observed in the lateral stress along 22 direction in X-ray measurement.

Thus, both FEM simulation and X-ray measurement shows the same trend for compressive and tensile stress distribution along different direction which is caused by the anisotropic characteristic of single crystal. It is found that the compressive residual stress is easier to generate in (001) direction than (111) and (110) direction, which is beneficial to the fatigue life improvement after μLSP.

3.4 Comprasion of residual stress between 2-D and 3-D deformation state

Followed the study of Chen et al. in 2003, the deformation state is approximately two dimensional if one shocked line is applied on sample surface. The lateral residual stress (S11) distribution on the cross section of the shocked line from 2-D FEM simulation is shown in Fig. 12(a), the compressive residual stress is dominate near the sample surface (0~40μm below the surface) while the tensile stress is found concentrated at the deeper level. Fig. 12(b) shows the distribution of residual stress σ11 in 3-D FEM simulation. In order to do the comprasion, the crystal orientation of 1, 2, 3 is the same in 2-D and 3-D simulation. In the 12 cross section, 3-D simulation shows that the tensile residual stress is small compared with the compressive stress and most tensile stress exists in 23 cross section instead of the bottom of 12 cross section.

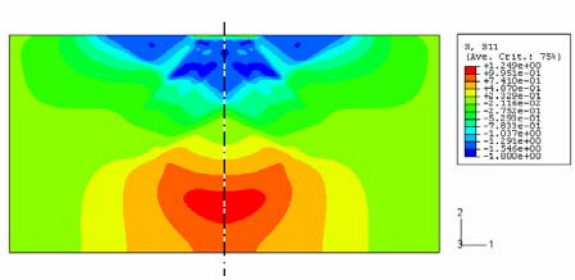

(a)

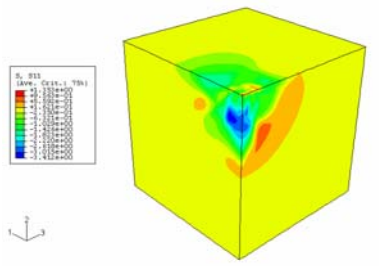

(b)

Fig. 12 Residual stress comparison between 2-D and 3-D simulation.
(a) S11 in 2-D simulation, 200×100μm (b) s11 in 3-D simulation, only quarter of the sample is simulated due to symmetry along 1 and 3 axis, 100×100×100μm

3.5 Lattice rotation field from simulation

Through FEM analysis of material response under μLSP with single crystal plasticity, the lattice rotation distribution can be simulated and compared with the EBSD measurement result.

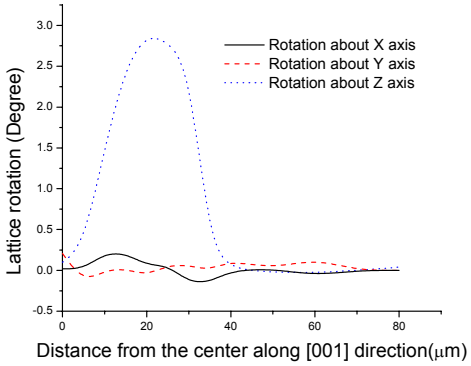

(a)

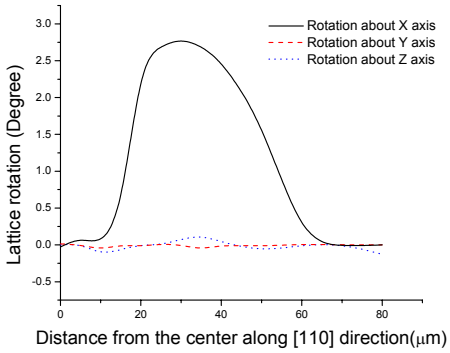

(b)

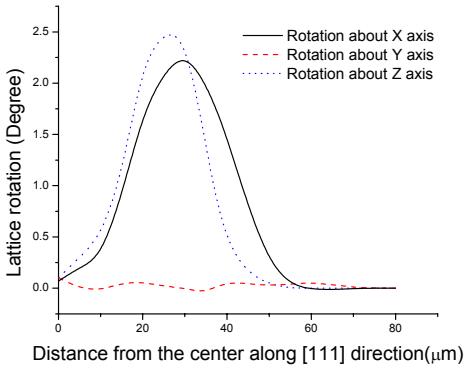

(c)

Fig. 13 Lattice rotation along the three axis on Al(110) sample surface

Fig. 13 (a-c) shows the lattice rotation around the X, Y and Z axes along different directions (<001>, <110>, <111>) on sample surface. Due to the crystalline symmetric, only one quarter of sample is shown here. The pattern is similar with that in Fig. 8 (a-c) except only half region is shown here. From the simulation, it is clear that the lattice rotation is mainly around X and Z axis while very small around Y axis which is the surface normal. Those results are consistent with the EBSD measurement in Fig. 8. The lattice rotation close to center of shocked region is near zero, when moving away from the

center, the rotation increases to a maximum value, then decreases again. The significant lattice rotation (>1 degree) occurs at 10um~60um in <110> direction and 10μm~40μm in <001> direction. The affect region along <111> direction is between the other two directions, which is from 10um to 50μm. Thus, the lattice rotation is not axisymmetric about the shock center which is caused by the anisotropic characteristic of single crystal.

3.6 Length scale effects consideration

It is believed that in the scale of a few to a few tens of microns, the conventional plasticity theory needs to be reexamined due to the "length scale effect". At this scale, strain gradient effects may be large enough to generate a significantly large density of geometrically necessary dislocations which will increase the flow stress in plastic deformation. According to the strain gradient theories of plasticity [15],

$$\tau = \alpha\mu b\sqrt{\rho_T} = \alpha\mu b\sqrt{\rho_S + \rho_G} \quad (4)$$

Where τ is the flow stress, μ is shear modulus, b is the Burger's vector, ρ_T is the total dislocation density, ρ_G is the geometrically necessary dislocation density and ρ_S is the statistically stored dislocation density. The ρ_G is related to the deformation state by

$$\eta = \rho_G b\,,\quad \eta = \frac{\partial \phi}{\partial x} \quad (5)$$

where η is the curvature of the crystal lattice. Therefore, geometrically necessary dislocations are those required to support a particular curvature in the crystallographic lattice at any given point in a deformed material. The lattice curvature is defined as the gradient of crystal lattice rotation dislocation and is given by a non-symmetric 2nd order tensor. Generally, it is very difficult to measure all nine components of the lattice curvature tensor. However, it is possible to make an order of magnitude estimate of the lattice curvature, and hence ρ_G. Thus, it is possible to estimate the strain gradient $\eta_x = \frac{\partial \alpha}{\partial x}$, $\eta_z = \frac{\partial \gamma}{\partial z}$ along different direction from Fig. 8(a) and (b). Thus, after obtaining the lattice rotation field, we can estimate the strain gradient along different crystalline direction and make it possible in the future to study the length effect in different crystal directions in μLSP. The average lattice curvature within the shock region can be estimated as a 5^0 lattice rotation over 50 μm, as in Fig 8, which gives $\eta \approx 1.5\times10^3\, m^{-1}$. With a Burger's vector of $2.5\times10^{-10}\, m$, the resulting density of geometrically necessary dislocation has the order of magnitude $\rho_G \approx 10^{13}\, m^{-2}$. The total dislocation density of a highly deformed metal is typically $\rho T \approx 10^{15}\, m^{-2}$, so plasticity length scale affects may not play the dominant role in laser shock peening.

3.7 Comparison of lattice rotation between 2-D and 3-D simulation

In the study of [5], a single line shock peens caused an approximate 2-D deformation state along the shock line direction. The in-plane lattice rotation was simulated using single crystal plasticity FEM on a cross section of the shock line in 2-D plane strain condition. As seen in Fig. 14 (a), the in-plane (1-2 plane) lattice rotation is around 4 degree with no out-of-plane lattice rotation. Three dimensional FEM simulation results under identical conditions are shown in Fig. 14(b); for which the 1-2 plane has the same orientation as the 2-D simulations. The in-plane-lattice rotation is around 3 degree and the pattern is similar with that in 2-D case. Although the out-of-plane lattice rotation (10^{-3} degree) is not zero, the lattice rotation field can still be considered as being approximated plane deformation.

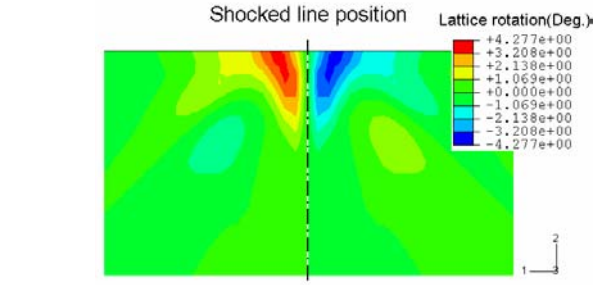

(a)

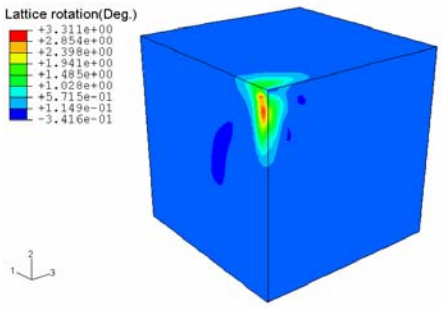

(b)

Fig. 14 Lattice rotation fields for Al(110) sample
(a) 2D simulation , 200×100μm
(b) 3D simulation , 100×100×100μm

4. CONCLUSIONS

In this study, 3-D plastic deformation induced by microscale laser shock peening on single crystal Aluminum (110) surface was investigated with X-ray microdiffraction, EBSD, AFM and 3-D FEM simulation based on single crystal plasticity. The laser beam size is 12um with intensity at 4GW/cm^2. AFM measurement show the plastic deformation region is larger in [001] direction ±60μm along <001> direction and than <110> direction ±25μm with depth around 2μm which is consistent with the FEM result. The spatial distribution of residual stress state in shocked region was measured by X-ray microdiffraction and the compressive residual stress is estimated to as large as up to –120MPa was found in an ellipse indentation region 50x80μm near the center and tensile stress was estimated to be up to +90MPa near the outer edge of indentation. The plastic deformation, compressive residual stress is most significant along [001] direction while the tensile stress is more concentrated in [110] direction. 3-D FEM simulation shows similar residual stress distribution as X-ray measurement. EBSD measurement and 3-D FEM simulation both show that the lattice rotation is around 3 degree up to

50μm away, from the shock center. The lattice rotation distribution along different crystal direction make it possible to estimate the length effect dependence on crystal orientation. Compared with 2-D plastic deformation in line shock condition, the tensile stress is closer to the sample surface in 3-D FEM simulation and lattice rotation is still under plane strain condition along the [001] across the shocked center.

The experimental methodology and results presented herein enable a systematic study of the micro scale laser shock peening process. It is now possible to systematically measure and simulate the extent and character of three dimensional plastic deformation, residual stresses and crystal lattice rotation fields with micron spatial resolution. Thus, the anisotropic plastic behavior of the single crystal under μLSP can be studied and these simulations will lay the ground work for more realistic simulations.

ACKNOWLEDGMENTS

This work is supported by the National Science Foundation under grant DMI-02-00334. JWK would like acknowledge support by the National Science Foundation under the Faculty Early Career Development (CAREER) Program with grant CMS-0134226. Guidance in X-ray microdiffraction provided by Dr. I. Cev Noyan and Dr. Jean Jordan-Sweet is appreciated.
.

REFERENCES

[1] Zhang, W. and Yao, Y. L., "Improvement of Laser Induced Residual Stress Distributions via Shock Waves," *Proc. ICALEO'00, Laser Materials Processing*, Vol. 89, pp. E183-192, 2000a.

[2] Zhang, W. and Yao, Y. L., "Micro Scale Laser Shock Processing of Metallic Components," *ASME Journal of Manufacturing Science and Engineering*, Vol. 124, No. 2, pp. 369-378, 2000b

[3] Chen, H. Q., and Yao, Y. L., "Modeling Schemes, Transiency, and Strain Measurement for Microscale Laser Shock Processing", *SME Journal of Manufacturing Processes*, to appear, 2003a.

[4] Zhang, W. and Yao, Y. L., "Feasibility Study of Inducing Desirable Residual Stress Distribution in Laser Micromachining," *Transactions of the North American Manufacturing Research Institution of SME* (*NAMRC XXIX) 2001,* pp. 413-420, 2001.

[5] Chen, H. Q., Yao, Y. L. and Kysar, J. W., "Spatially Resolved Characterization of Residual Stress Induced by Micro Scale Laser Shock Peening," *ASME Journal of Manufacturing Science and Engineering*, to appear, 2003b.

[6] Ungar, T., *et al.*, "X-ray Line-Broadening Study of the Dislocation Cell Structure in Deformed [001]-Orientated Copper Single Crystals", *Acta ,etall.*, Vol. 32, No. 3, pp. 332-342, 1984.

[7] Kysar, J. W., and Briant, C. L., "Crack Tip Deformation Fields In Ductile Single Crystals," *Acta Materialia*, Vol. 50, pp. 2367-2380, 2002.

[8] El-Dasher, B.S., et al., "Viewpoint: experimental recovery of geometrically necessary dislocation density in polycrystals", *Scripta Materialia*, Vol. 48, pp. 141-145, 2003.

[9] S. Zaefferer, et al., "On the influence of the grain boundary misorientation on the plastic deformation of aluminum bicrystals", *Acta Materialia*, Vol. 51, No. 16, pp. 4719-4735, 2003.

[10] Cullity, B. D., Elements of X-ray Diffraction, London, Addison-Wesley Publishing Company, Inc., Second edition, pp. 13-20, 1978.

[11] Asaro, R.J., "Micromechanics of Crystals and Polycrystals", *Advances in Applied Mechanics*, Vol. 23, pp. 1-115, 1983.

[12] Huang, Y., "A User-Material Subroutine Incorporating Single Crystal Plasticity In the ABAQUS Finite Element Program, Mech Report 178", Division of Applied Sciences, Harvard University, Cambridge, MA, 1991.

[13] Kysar, J.W., Addendum to "A User- Material Subroutine Incorporating Single Crystal Plasticity In the ABAQUS Finite Element Program, Mech Report 178", Division of Engineering and Applied Sciences, Harvard University, Cambridge, MA, 1997.

[14] Rice, J. R., "Tensile Crack Tip Fields In Elastic-Ideally Plastic Crystals," *Mechanics of Materials,* Vol. 6, pp. 317-315, 1987.

[15] Gao, H., et al., "Mechanism-based strain gradient plasticity- I. Theory", *Journal of the mechanics and Physics of Solids*, Vol. 47, pp. 1239-1263, 1999.

